RESEARCH ARTICLE

Key Points:
- A new algorithm for retrieving sea ice emissivities at microwave frequencies
- The spectral emissivity slope between 10.6 and 18.7 GHz was devised as a means of differentiating between first-year and multiyear sea ice

Correspondence to:
B-J. Sohn,
sohn@snu.ac.kr

Differentiating between first-year and multiyear sea ice in the Arctic using microwave-retrieved ice emissivities

Sang-Moo Lee[1], Byung-Ju Sohn[1] (iD), and Seong-Joong Kim[2]

[1]School of Earth and Environmental Sciences, Seoul National University, Seoul, South Korea, [2]Division of Polar Climate Change Research, Korea Polar Research Institute, Incheon, South Korea

Abstract Polarized emissivities of the sea ice over the Arctic were retrieved at Advanced Microwave Scanning Radiometer–EOS 10.65, 18.7, 23.8, and 36.5 GHz channel frequencies. Results indicate that retrieved emissivities are consistent with other emissivity estimates. However, errors in the retrieved emissivity for multiyear sea ice at 23.8 and 36.5 GHz can be large up to 8% and 20%, respectively, because of ignoring the freeboard ice scattering and the use of the same emission layer as in 6.925 GHz. It is shown that the emissivity slope for first-year ice between 10.65 and 18.7 GHz is opposite to that for multiyear sea ice, enabling a distinction between first-year ice and multiyear ice. Using these differences in spectral features with ice types, an emissivity difference (vertically polarized emissivity difference between 10.65 and 18.7 GHz) was devised to differentiate between first-year sea ice and multiyear sea ice. A comparison with the ice status information obtained from Cold Regions Research and Engineering Laboratory buoy measurements demonstrates that the method can separate first-year ice from multiyear ice, implying that this technique enables us to obtain instantaneous and pixel-level ice-type information from space-based passive microwave measurements.

1. Introduction

Successful monitoring of sea ice over the polar regions over last three decades owes much to the advent of satellite multichannel microwave (MW) radiometer measurements. Although in recent years applications of the MW radiometer measurements have been expanded to cover diverse areas, derived parameters have been limited to a few variables such as the sea ice concentration [*Comiso et al.*, 2003; *Zhang et al.*, 2013] and ice types [*Fowler et al.*, 2004; *Maslanik et al.*, 2011; *Comiso*, 2012]. However, considering the importance of the Arctic in the global climate change and long-term weather forecasting, as exemplified in the Arctic Oscillation [*Wu and Wang*, 2002] or Arctic amplification [*Francis and Vavrus*, 2012], observations of other geophysical parameters are much demanded.

In particular, sea ice emissivity is an important parameter. Poor emissivity information is one of the main reasons why satellite data are not much used for weather forecasting over the polar regions. But, emissivity retrieval is difficult because it is tied with surface temperature to determine the amount of radiation emitted from the surface. It appeared not possible to retrieve surface temperature and emissivity simultaneously from space without knowing one of two variables before measuring the other. However, it has been demonstrated that both parameters could be simultaneously retrieved without such a priori information [*Lee and Sohn*, 2015] from the use of low-frequency 6.925 GHz microwave measurements based on the analytically driven "combined Fresnel equation" [*Sohn and Lee*, 2013]. Unfortunately, the method may be difficult to apply for higher MW frequencies because of the roughness effect of the sea ice on the Fresnel assumption employed for 6.925 GHz. In order to circumvent such caveats, in this study, we use the 6.925 GHz results for determining the emissivities at higher frequencies. We assume that the physical temperature obtained at 6.925 GHz can be used as the physical surface temperature for other lower frequencies. A detailed explanation on the algorithm itself is provided in section 2.

There have been efforts to differentiate ice types such as first-year and multiyear sea ice, based on the use of the microwave satellite imagery [*Comiso*, 1990; *Comiso*, 2012]. *Breivik and Eastwood* [2009] developed an ice-type classification method using passive microwave data, in combination with scatterometer observations, using a Bayesian approach. Another algorithm using the microwave measurements to determine the multiyear sea ice concentration has been developed by the NASA Team for the Special Sensor for

Microwave Imager (SSM/I) measurement [*Cavalieri et al.*, 1991]. This so-called NASA Team algorithm needs tie points (i.e., typical brightness temperature or emissivity values for first-year ice, multiyear ice, and open water) [*Andersen*, 1998]. But, the algorithm has been primarily used for determining the sea ice concentration without validating the fixed tie point value for multiyear sea ice. Nonetheless, sea ice-type data are potentially important for validating model outputs and monitoring the climate change over the Arctic [*Jahn et al.*, 2012; *Ye et al.*, 2016].

Despite their success, those algorithms seem to be prone to uncertainties, due to the nature of statistical or tie-point algorithm, although improvement has been made using tie points for multiyear sea ice dynamically varying with season and location [*Comiso*, 2012; *Ivanova et al.*, 2015; *Ye and Heygster*, 2015]. In this study, different from statistical or tie-point approach, we attempt to devise a more physics-based method to differentiate between first-year sea ice and the multiyear sea ice.

2. Emissivity Retrieval From Lower Frequency Microwave Measurements

In this study, the MW frequencies we are working with are limited for lower frequencies (i.e., here 10.65, 18.7, 23.8, and 36.5 GHz Advanced Microwave Scanning Radiometer (AMSR) channel frequencies) because sea ice temperature obtained at AMSR 6.925 GHz (hereafter referred to as 6.9 GHz) is used as a sea ice-snow interface temperature for other channels in interest.

2.1. Algorithm

In the spaceborne MW remote sensing, the observed polarized brightness temperature, $T_p(v)$, under nonscattering plane-parallel atmospheric conditions can be expressed by

$$T_p(v) = \varepsilon_p(v)T_s e^{-\tau(v)} + T_{p,\text{up}}(v) + \left(1 - \varepsilon_p(v)\right)T_{p,\text{down}}(v)e^{-\tau(v)} \qquad (1)$$

where v and p are frequency and polarization state, ε_p and T_s are polarized emissivity and surface temperature, τ is the total atmospheric optical thickness, and $T_{p,\text{up}}(v)$ and $T_{p,\text{down}}(v)$ are upwelling and downwelling brightness temperatures vertically integrated over the entire atmosphere above the ice surface. Equation (1) can be rearranged for $\varepsilon_p(v)$, i.e.,

$$\varepsilon_p(v) = \frac{T_p(v) - T_{p,\text{up}}(v) - T_{p,\text{down}}(v)e^{-\tau}}{\left(T_s - T_{p,\text{down}}(v)\right)e^{-\tau}} \qquad (2)$$

Thus, when $T_{p,\text{up}}(v)$, $T_{p,\text{down}}(v)$, $\tau(v)$, and T_s are known, the polarized surface emissivity at the frequency v can be determined from the measured brightness temperature $T_p(v)$.

Even though *Lee and Sohn* [2015] method allows to determine T_s from satellite-measured brightness temperatures, it is difficult to use the method for higher frequencies. It is because the sea ice roughness effect becomes substantial at higher frequencies to apply the combined Fresnel relationship [*Sohn and Lee*, 2013]. In this study, instead of correcting the roughness effect for higher-frequency channels we use 6.9 GHz-derived T_s for the surface temperature at other frequencies. For a given T_s, the emissivity can be determined by explicitly taking account of atmospheric contribution terms in equation (2) at a given frequency, which can be calculated using a radiative transfer model with given atmospheric temperature and moisture profiles. In this calculation, the Radiative Transfer for TOVS (RTTOV) model is used with atmospheric profiles obtained from Interim European Centre for Medium-Range Weather Forecasts (ECMWF) Re-Analysis (ERA-Interim) data. At this point, equation (2) is solved for the emissivity.

2.2. Uncertainty Analysis

Here because the method only deals with the upwelling radiance leaving the surface, the radiative transfer elements associated with snow and ice such as frequency-dependent emission layer, scatterings due to the freeboard sea ice, are not explicitly counted. In this section, possible errors in the estimated emissivity are examined.

2.2.1. Influences of Uncertain Atmospheric Profiles

As shown in equation (2), emissivity retrievals are influenced by atmospheric conditions on the microwave absorbing/emitting gases. Atmospheric hydrometeor is certainly an error source despite lower frequencies dealt in this study. Fortunately, though, hydrometeors in the Arctic polar atmosphere may not be a big issue because of very small amount of water vapor and weak updraft motion particularly over the sea ice covered

Table 1. Profiles of Density, Exponential Correlation Length, and Salinity of Snow and First-Year Ice[a]

Layer No.	Layer Depth (m)	Density (kg/m^3)	Exponential Correlation Length (mm)	Salinity (Ppt)
1	0.00–0.07	260	0.07	0
2	0.07–0.12	410	0.10	0
3	0.12–0.13	300	0.14	0
4	0.13–1.15	920	0.15	7

[a]Adapted from *Mätzler* [2006].

region in interest. Since the reanalysis data carry substantial errors in the polar region, uncertainty in the retrieved emissivity can be expected. However, considering that the atmospheric absorption of microwave radiation in the frequencies lower than 36.5 GHz is small except for the weak water vapor absorption band around 22.235 GHz, errors caused by uncertain atmospheric profiles should be small. Furthermore, moisture content over the Arctic is very small due to the extremely cold conditions, leading to the expectation that the uncertainty influences should be small enough to ignore.

Nonetheless, we take a sensitivity test of examining how the retrieved emissivities are sensitive against uncertain atmospheric conditions. *Jakobson et al.* [2012] reported that the bias and root-mean-square error (RMSE) of ERA-Interim temperature (humidity) profiles over the Arctic are about 2.5 K (7%) and 1.9–3 K (15%), respectively. From the sensitivity test of allowing ±5.5 K error (bias plus RMSE) in the all layers of ERA-Interim daily mean temperature profiles over the Arctic (January 2010), the induced uncertainty level in the emissivity is on the order of 10^{-3}. Uncertainty influence from humidity profile (allowing 30% errors) appears to be even more negligible.

2.2.2. Influences of Snow and Ice Scatterings

Scatterings by snow and freeboard ice can be error sources for the sea ice emissivity retrieval, especially for the multiyear ice. Scattering effects by the snow and freeboard ice are counted and then estimated using the Microwave Emission Model for Layered Snowpacks (MEMLS) model for the sea ice [*Mätzler*, 2006; *Tonboe et al.*, 2011]. Snow/ice properties for the first-year and multiyear ice profiles (Tables 1 and 2) are obtained from *Mätzler* [2006], based on *Tonboe and Andersen* [2004] for the first-year ice and from field observations taken during the Norwegian Remote Sensing Experiment for multiyear sea ice.

The MEMLS-estimated light depletions (given in percentage) due to the scatterings of snow and freeboard ice are given in Table 3. It is shown that influences of snow layers over both first-year ice and multiyear ice are small for the lower frequencies, while small increases in the depletion are noted for higher frequencies, causing nonnegligible scattering for 36.5 GHz (about 2.25%) related to the multiyear sea ice. In addition, depletion rates are calculated with extreme snow conditions (i.e., snow depth = 34 cm and snow density = 360 kg m^{-3}), which are maximum values of climatological snow properties provided in *Warren et al.* [1999]. Results for the extreme snow cases showed that depletions are not much discernible from results in Table 3, confirming that the snow depth over the Arctic sea ice is generally thin enough to ignore the snow impact at lower MW frequencies [*Andersen et al.*, 2007; *Mathew et al.*, 2009].

For the freeboard ice, light depletions at 6.9, 10.65, 18.7, 23.8, and 36.5 GHz channels are about 0.06%, 0.28%, 0.99%, 3.56%, and 14.43%, respectively. The depletion rate is against the upwelling radiation at the bottom of the freeboard ice. It is noted that scattering influences of the freeboard ice are comparatively large for

Table 2. Same as in Table 1 Except for Multiyear Sea Ice[a]

Layer No.	Layer Depth (m)	Density (kg/m^3)	Exponential Correlation Length (mm)	Salinity (Ppt)
1	0.00–0.07	260	0.07	0
2	0.07–0.08	450	0.10	0
3	0.08–0.10	300	0.10	0
4	0.10–0.11	450	0.10	0
5	0.11–0.16	300	0.10	0
6	0.16–0.17	450	0.10	0
7	0.17–0.19	300	0.14	0
8	0.19–0.29	750	0.25	0.5
9	0.29–2.49	900	0.20	2.5

[a]Adapted from *Mätzler* [2006].

Table 3. Light Depletion Rate (%) due to the Scattering by Snow and Freeboard Ice

Types	6.9 GHz	10.7 GHz	18.7 GHz	23.8 GHz	36.5 GHz
Snow (first-year ice)	0.04	0.13	0.67	0.92	1.91
Snow (multiyear ice)	0.09	0.30	0.94	1.00	2.25
Freeboard ice	0.06	0.28	0.99	3.56	14.43

23.8 GHz and 36.5 GHz, and thus, the retrieved emissivity at 36.5 GHz can be subject to a substantial error (14.43%) if the scattering is not counted. On the other hand, scattering influences on the light depletion are less than 1% for 6.9, 10.65, and 18.7 GHz channels.

2.2.3. Influences of the Same Ice Emission Layer

In this study, 6.9 GHz-derived T_s is used for replacing T_s in equation (2) for other higher frequencies (here 10.65, 18.7, 23.8, and 36.5 GHz). However, because the emission layer should vary with frequency, we expect errors caused by the assumption that emission layers are same in the lower frequencies. In order to examine the influences of assumed same interface temperatures across 6.9–36.5 GHz channels, we first examine where the emitting layers are located, using weighting functions to the emitting radiation at the snow top. In this calculation, only emission is considered with ice profiles given in Tables 1 and 2. Vertical distributions of the weighting functions obtained from MEMLS for the first-year and multiyear ice are given in Figure 1. Also obtained are emitted temperatures (TB_e) at the snow top from following equation,

$$TB_e = \frac{\int_d^0 T(z)\,W(z)\,dz}{\int_d^0 W(z)\,dz} \tag{3}$$

where $T(z)$ and $W(z)$ are temperature and weighting function at depth z, respectively, and d is the depth of the ice bottom. Unity emissivity is assumed at each layer. In this calculation, averaged temperature profiles of snow and ice layers from Cold Regions Research and Engineering Laboratory (CRREL) buoy measurements in January 2011 are used.

Weighting functions for the first-year sea ice show that the emitting layers are located in a shallow layer of about 5 cm in depth just below the snow layer. The calculated emitting temperatures for the 6.9, 10.65, 18.7, 23.8, and 36.5 GHz are 253.3, 252.8, 252.3, 252.2, 252.0 K, respectively, supporting the notion that the emission layer is nearly frequency-independent between 6.9 and 36.5 GHz for the first-year ice [*Comiso et al.*, 2003].

Different from the first-year case, a much broad distribution of the weighting function is noted for 6.9 GHz with a peak around 50 cm in depth, and it shows that the emission signal can originate from even a fairly
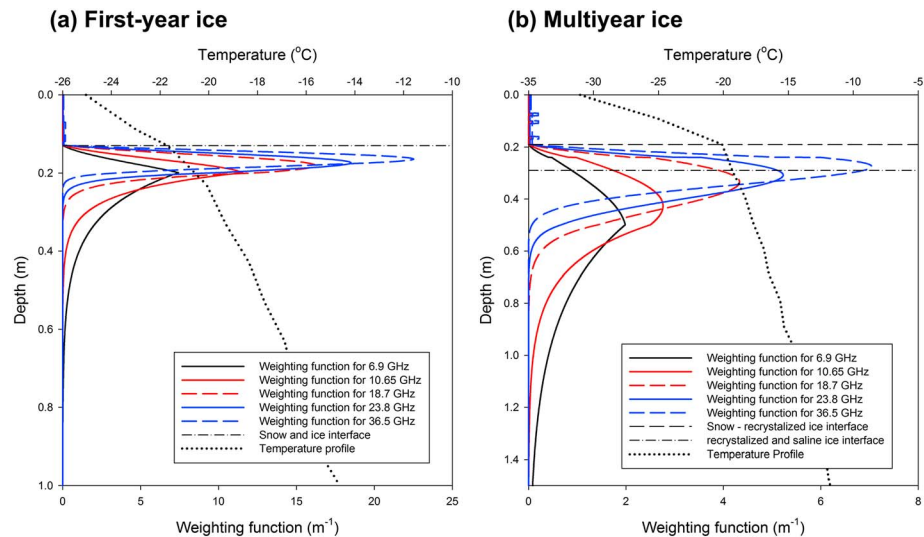

Figure 1. Calculated weighting functions of AMSR low-frequency channels, i.e., 6.9 (black lines), 10.65 (red lines), 18.7 (red dashed lines), 23.8 (blue lines), and 36.5 GHz (blue dashed lines), for (a) first-year ice and (b) multiyear ice. Temperature profiles for first-year ice and multiyear ice are also given (dotted lines).
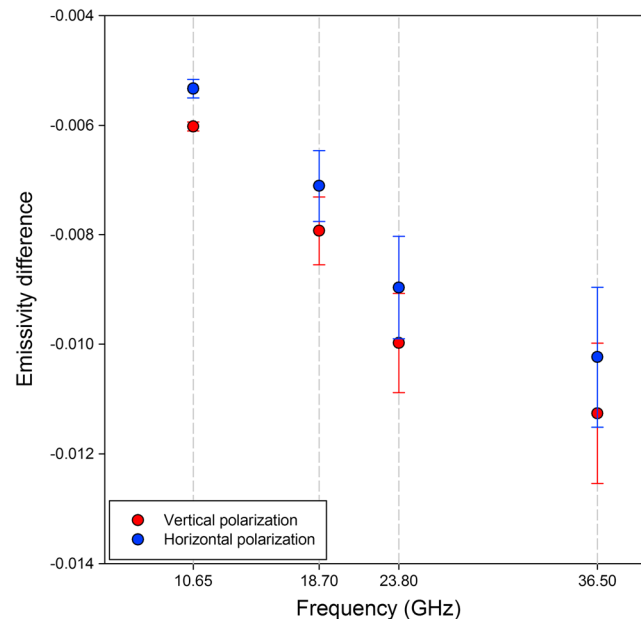
Figure 2. Emissivity error caused by the use of the same emission layers. The red and blue dots are for vertically and horizontally polarized component, respectively. The associated vertical bar represents a corresponding one standard deviation.

deeper layer up to 1.5 m. With higher frequencies, the emission layers are located in shallower layers. Such different shapes and peaks imply a difficulty of using 6.9 GHz-derived temperature for other channels. The calculated TB_e at 6.9, 10.65, 18.7, 23.8, and 36.5 GHz for the multiyear sea ice are 256.5, 255.3, 254.5, 254.2, and 253.9 K, respectively, causing -1.2, -2.0, -2.3, and -2.6 K differences for 10.65, 18.7, 23.8, and 36.5 GHz channels, compared to the 6.9 GHz value (i.e., 256.5 K). With the calculated emitted temperature differences, the uncertainty of the T_s assumption is tested, allowing uncertainties of -1.5 K for 10.65 GHz, -2.0 K for 18.7 GHz, -2.5 K for 23.8 GHz, and -3.0 K for 36.5 GHz channels. The test shows that emissivity differences for vertical (horizontal) polarization are -0.0060 (-0.0053), -0.0079 (-0.0071), -0.0100 (-0.0089), and -0.0112 (-0.0102) for 10.65, 18.7, 23.8, and 36.5 GHz, respectively, which are less than 1% error in the lower frequencies below 18.7 GHz (Figure 2). However, similar to the scattering influences, error influences caused by the use of the same emission layer appear to be larger for 23.8 GHz and 36.5 GHz channels.

2.2.4. Overall Uncertainties

Putting it all together, we examine the possible uncertainties in the retrieved emissivities, caused by uncertain atmospheric profiles, neglected snow and freeboard sea ice scattering, and the assumed same emission layer. In doing so, Advanced Microwave Scanning Radiometer–EOS (AMSR-E) channel brightness temperatures are simulated using MEMLS model plus RTTOV model, with and without those error sources, and then emissivities are retrieved from two sets of simulated brightness temperatures (i.e., with/without error sources).

Differences in emissivities retrieved from those two sets of simulated brightness temperatures are given in Figure 3. It shows that emissivity differences for vertical (horizontal) polarization are about -0.0092 (-0.0091), -0.0199 (-0.0185), -0.0567 (-0.0522), and -0.1546 (-0.1432) for 10.65, 18.7, 23.8, and 36.5 GHz, respectively. It is noted that emissivities at the frequencies below 18.7 GHz can be retrieved with an error up to 2%. On the other hand, emissivity errors become larger up to 8% and 20% for 23.8 and 36.5 GHz, respectively, and these are found to be mostly from the freeboard ice scatterings. Because of these error analysis results, we use 10.65 and 18.7 GHz emissivities for differentiating between first-year sea ice and multiyear sea ice.

3. Used Data

In this study, AMSR-E ascending/descending level 3 daily brightness temperatures are used, in conjunction with the sea ice concentration to remove the scenes contaminated by the open water. Brightness
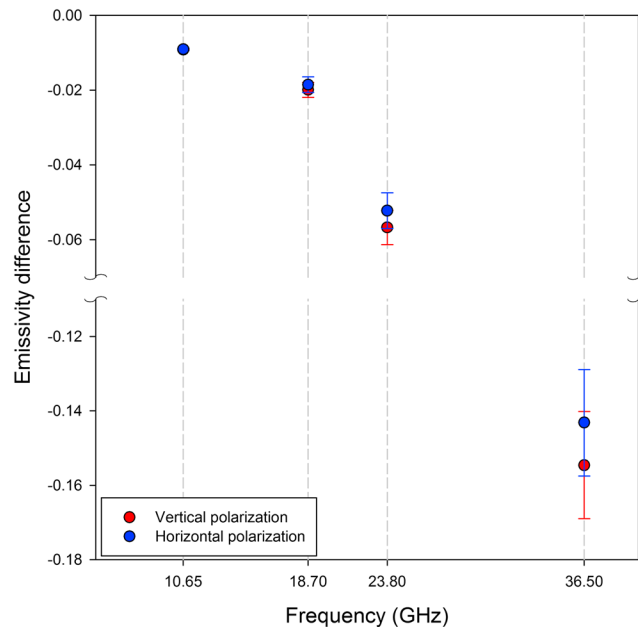
Figure 3. Same as in Figure 2 except for the total uncertainties.

temperatures and sea ice concentration in the 25 km × 25 km grid format are obtained from the Global Change Observation Mission (GCOM) Web site (http://gcom-w1.jaxa.jp/).

Calculating atmosphere-related components in equation (2), we use 6-hourly ERA-Interim data, which are in the 0.75° × 0.75° grid format [*Dee et al.*, 2011; http://apps.ecmwf.int/datasets/data/interim_full_daily]. We also take a simple average of 6-hourly ERA-Interim data for the daily mean. Because of different spatial scales, the collocated ERA-interim temperature and humidity profiles are obtained by finding the nearest ERA-Interim data point from AMSR-E data point in interest.

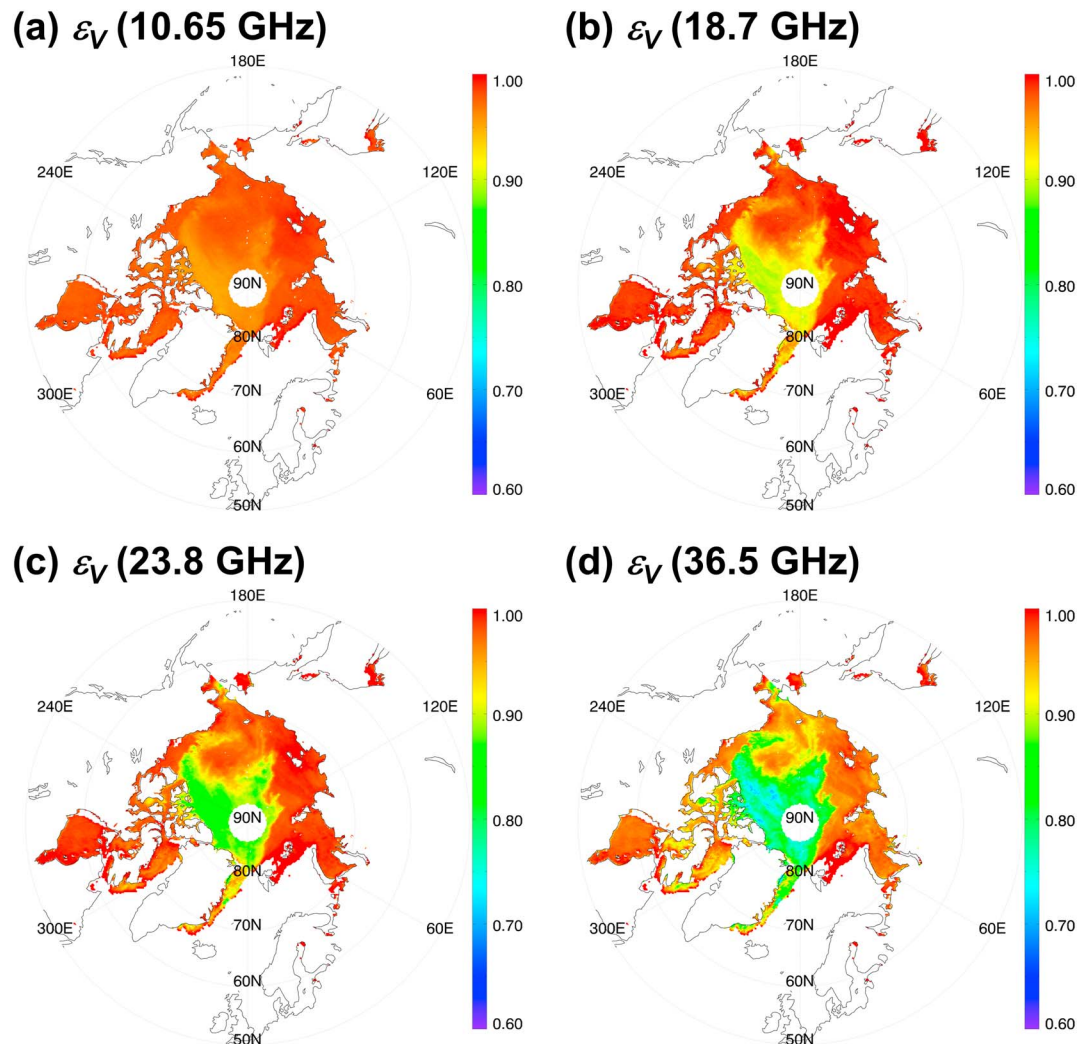To validate whether the technique is capable of discriminating between first-year and multiyear sea ice, we use CRREL Ice Mass Balance (IMB) buoy data [*Polashenski et al.*, 2011; *Perovich et al.*, 2013], downloaded from the CRREL web page (http://imb-crrel-dartmouth.org/imb.crrel/buoysum.htm). The CRREL IMB data provide the ice-type (i.e., first-year or multiyear) at the initial time of buoy deployment. Since the comparison is made for January, we assume that the ice-type (first-year or multiyear) reported in the CRREL IMB data is maintained along the drifting track during January.

Also compared with obtained sea ice-type are the sea ice age from the National Snow and Ice Data Center (NSIDC) [*Anderson et al.*, 2014], the OSI-SAF (Ocean and Sea Ice-Satellite Application Facilities) sea ice-type [*Breivik and Eastwood*, 2009], and the multiyear ice concentration from AMSR-E measurements [*Hao and Su*, 2015]. The NSIDC ice age data are derived from sea ice motion vectors [*Fowler et al.*, 2013], which are obtained by merging ice motions from satellite-based infrared and MW images, buoy measurements, and reanalysis data. Data sets are available from the NSIDC Web site (http://nsidc.org/data/docs/measures/nsidc-0532/). The OSI-SAF products provide the first-year and multiyear sea ice-type [*Breivik and Eastwood*, 2009] and are available from the Web site (http://osisaf.met.no/p/ice/). Originally, the NASA Team algorithm using 19 GHz and 37 GHz brightness temperatures has been developed for Special Sensor Microwave Imager (SSM/I) measurements. But, in this study, the SSM/I algorithm [*Cavalieri et al.*, 1991] is directly used for obtaining the multiyear sea ice concentration from AMSR-E measurements.

4. Results

4.1. Polarized Sea Ice Emissivities

Figures 4 and 5 show the geographical distributions of retrieved polarized emissivities of the sea ice at 10.65, 18.7, 23.8, and 36.5 GHz at the AMSR-E viewing angle (i.e., 55°) over the Arctic on 1 January 2010. It is noted that the horizontal component is geographically more variable than the vertical component. This is because the horizontal polarization is more sensitive to surface conditions such as ice status and surface process than the vertical polarization. Lower ε_V and ε_H values, in particular at higher frequencies, are found in the central Arctic and the Greenland Sea where multiyear sea ice is prevalent. Especially in the vertical component, the lower emissivity areas appear to contrast with higher values in surrounding areas, and this contrast seems to be more prominent at higher frequencies such as 36.5 GHz. Similar features of the geographical distribution and spectral dependency are also found in the horizontal component, but with a less clarity. It is of importance to note that retrieved polarized emissivities have a tendency to decrease with increasing frequency over the Arctic sea ice, which is consistent with the general trends found in other measurements (see also

Figure 4. Retrievals of vertically polarized emissivities over the Arctic Ocean for AMSR-E 10.65, 18.7, 23.8, and 36.5 GHz on 1 January 2010.

Figure 6 and Table 4). However, it should be mentioned, as shown in the error analysis, that uncertainties in the retrieved emissivity are substantial at 23.8 and 36.5 GHz channels.

Because of the lack of in situ emissivity measurements, long-term mean-retrieved emissivities, taken over the entire Arctic during January of 2003–2011, are compared with values available in the literature. Furthermore, we do this for first-year sea ice (or seasonal sea ice) and multiyear sea ice (older than 1 year) separately, based on the NSIDC ice age classification. Emissivities are compared separately for first-year ice and the remaining part (i.e., multiyear ice), because the emissivity distribution seems to roughly outline the boundary of the multiyear ice area, as noted in Figures 4 and 5. Thus, it is of interest to examine how the spectral dependency might vary between first-year sea ice and multiyear sea ice. Emissivity is taken into an average for each sea ice group only if the corresponding sea ice concentration is greater than 95%.

Nine-year averaged emissivities for the first-year sea ice and multiyear sea ice at 6.9, 10.65, 18.7, 23.8, and 36.5 GHz are shown in Figure 6. Emissivities reported in various publications are summarized in Table 4, along with averaged values of retrieved emissivities over the areas of NSIDC-determined first-year sea ice and multi-year sea ice. In Table 4, *Stroeve et al.* [2006] reported the emissivities for seasonal and multiyear ice estimated from a microwave model (called MicroWave radiative transfer MODel, MWMOD) with observed typical values of the sea ice property. The obtained emissivities were used for simulating AMSR-E brightness temperatures. *Mathew et al.* [2009] retrieved the sea ice emissivities from AMSR-E measurements with the use of ice
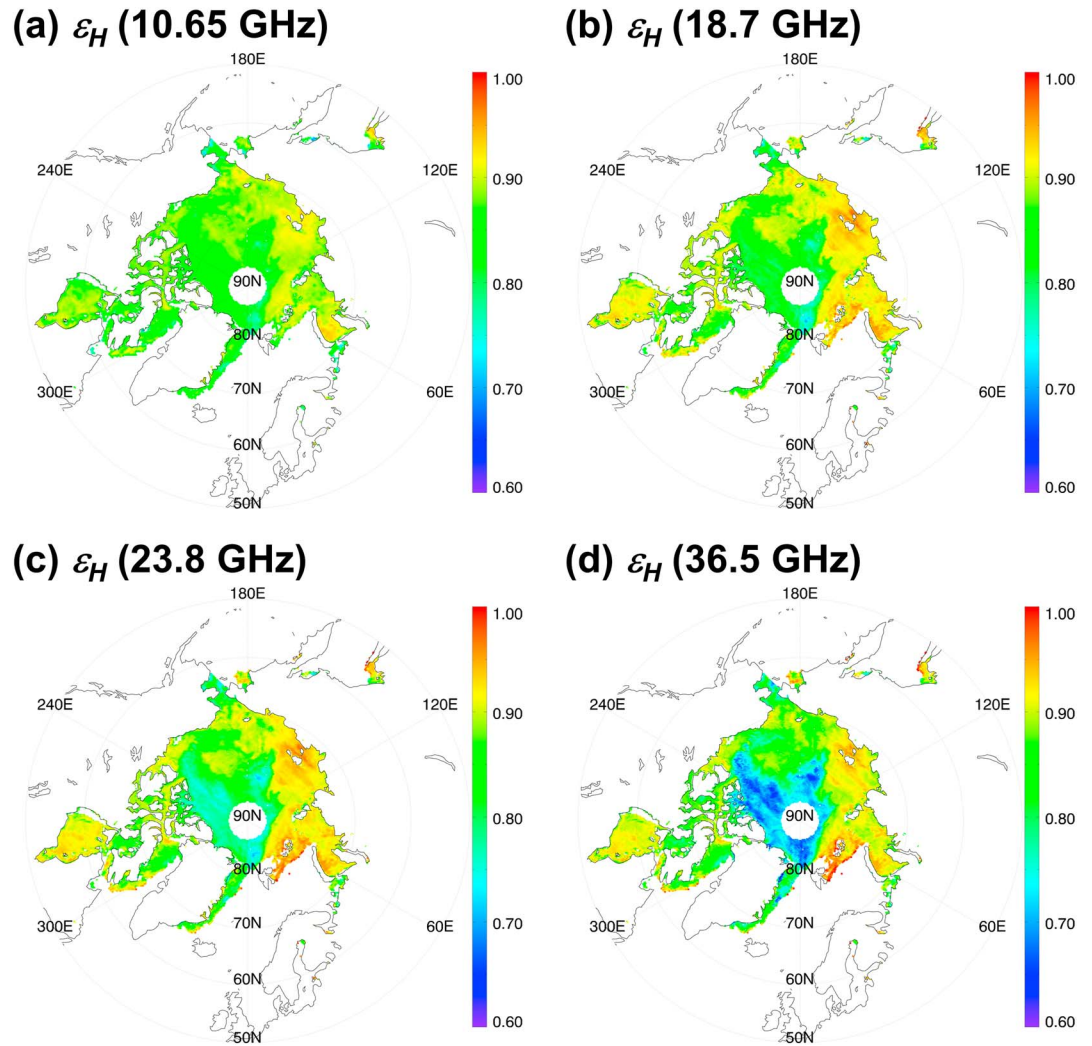
(a) ε_H (10.65 GHz)

(b) ε_H (18.7 GHz)

(c) ε_H (23.8 GHz)

(d) ε_H (36.5 GHz)

Figure 5. Same as in Figure 4 except for horizontally polarized emissivities.

(a) Vertically polarized emissivity
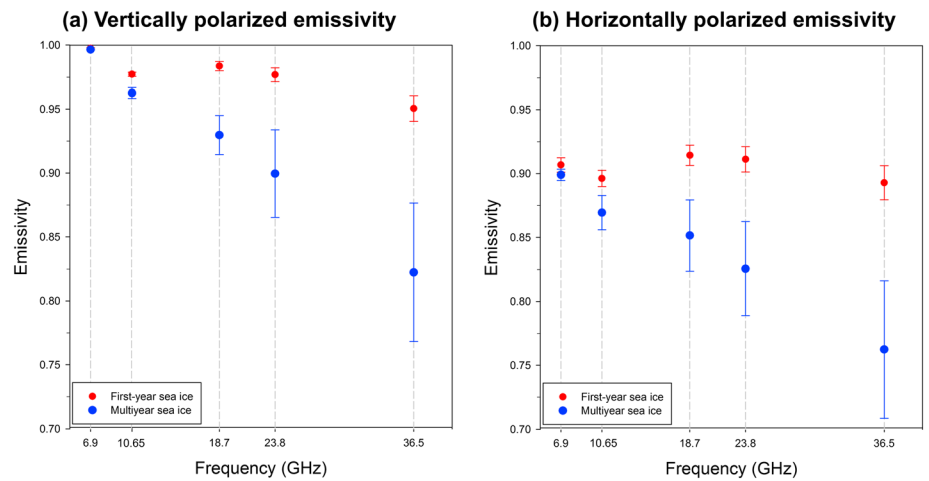
(b) Horizontally polarized emissivity

Figure 6. Nine-year (2003–2011) January mean (a) vertically polarized and (b) horizontally polarized emissivities averaged over the Arctic for first-year sea ice (red dots) and multiyear sea ice (blue dots). The vertical bar represents a one standard deviation.

Table 4. Referred and Retrieved Vertically Polarized Emissivities for the First-Year and Multiyear Sea Ice at 6.9, 10.65, 18.7, 23.8, and 36.5 GHz at a Viewing Angle of 55°

Frequency	References	ε_V (First-Year)	ε_V (Multiyear)	ε_H (First-Year)	ε_H (Multiyear)
6.9 GHz	*Mathew et al.* [2009]	0.960	0.968	0.872	0.873
	Stroeve et al. [2006]	0.983	0.980	0.847	0.920
	Campbell and Gloersen [1983]	0.990[a,b]	0.960[a,b]	–	–
	Comiso [1983]	0.930[a,b]	0.880[a,b]	0.870[a,b]	0.820[a,b]
	This study	0.997	0.996	0.906	0.899
10.7 GHz	*Mathew et al.* [2009]	0.959	0.944	0.880	0.954
	Stroeve et al. [2006]	0.989	0.960	0.878	0.940
	Comiso [1983]	0.930[a]	0.860[a]	0.880[a]	0.800[a]
	This study	0.977	0.962	0.896	0.869
18.7 GHz	*Willmes et al.* [2014]	0.946[a]	–	–	–
	Mathew et al. [2009]	0.970	0.894	0.899	0.822
	Stroeve et al. [2006]	0.991	0.880	0.937	0.830
	Andersen [1998]	0.950[c,d]	0.830[c,d]	0.890[c,d]	0.760[c,d]
	St. Germain [1993]	0.999[c,d]	0.918[c,d]	0.941[c,d]	0.839[c,d]
	Campbell and Gloersen [1983]	0.980[a,e]	0.800[a,e]	0.940[a,e]	0.800[a,e]
	Comiso [1983]	0.920[a,e]	0.860[a,e]	0.880[a,e]	0.750[a,e]
	This study	0.984	0.930	0.914	0.929
23.8 GHz	*Mathew et al.* [2009]	0.967	0.854	0.897	0.787
	Stroeve et al. [2006]	0.986	–	0.944	–
	Comiso [1983]	0.920[a,f]	0.770[a,f]	0.890[a,f]	0.740[a,f]
	This study	0.976	0.900	0.911	0.825
36.5 GHz	*Willmes et al.* [2014]	0.873	–	–	–
	Mathew et al. [2009]	0.951	0.762	0.882	0.703
	Stroeve et al. [2006]	0.981	0.880	0.948	0.800
	Haggerty and Curry [2001]	–	0.890[a]	–	0.840[a]
	Andersen [1998]	0.920[c]	0.700[c]	0.890[c]	0.650[c]
	St. Germain [1993]	0.979[c]	0.766[c]	–	–
	Campbell and Gloersen [1983]	0.960[a]	0.710[a]	0.920[a]	0.680[a]
	Comiso [1983]	0.920[a]	0.710[a]	0.880[a]	0.660[a]
	This study	0.950	0.822	0.893	0.762

[a]Emissivities for viewing angle of 50°.
[b]Emissivities at 6.6 GHz.
[c]Emissivities for viewing angle of 53.1°.
[d]Emissivities at 18.0 GHz.
[e]Emissivities at 19.3 GHz.
[f]Emissivities at 21.0 GHz.

temperature regressed from near surface temperature of ERA-Interim data and atmospheric correction, for the seasonal ice at one region and for multiyear ice at another region in January 2005. These values are used for generating interchannel emissivity correlations which are important factor in data assimilation. *Haggerty and Curry* [2001] obtained an aircraft-measured emissivity for the multiyear sea ice by combining with the IR-measured temperature near Barrow, Alaska, in late May 1998, to retrieve the amount of atmospheric hydrometeors. *Campbell and Gloersen* [1983] provided emissivities of tie points for SMMR (scanning multichannel microwave radiometer), and they were obtained by dividing SMMR radiances by the Arctic Ocean buoy-measured temperature. *St. Germain* [1993] provided emissivities of tie-points for SSM/I modified NASA Team algorithm. *Andersen* [1998] provided emissivities of tie points for SSM/I Danish algorithm, which was obtained from SSM/I radiances combined with National Centers for Environmental Prediction reanalysis surface temperatures. *Comiso* [1983] retrieved emissivity from the Nimbus-7 SMMR radiances combined with temperature-humidity infrared radiometer temperatures. It was used for the emissivity classification with respect to ice-type. *Willmes et al.* [2014] reported first-year sea ice emissivities calculated from the MEMLS simulations with physical properties of ice.

Emissivities at channels other than 6.9 GHz appear to have a similar tendency but with a large deviation among the measurements. Retrieved emissivities in this study seem close to *Stroeve et al.* [2006] and *Mathew et al.* [2009]. In contrast, emissivities of tie-points used for satellite algorithms and from the use of infrared-derived temperature (except for *St. Germain* [1993]) appear smaller than the retrieved emissivities

in this study as well as published values. In summary, except for 6.9 GHz and infrared-based emissivities, the retrieved emissivities seem to be in the range of the values reported in the literature.

Overall, emissivity values found in the literatures vary substantially, not providing a concrete consensus partly due to the used different methodologies and different geophysical parameters/meanings. Nevertheless, *Mathew et al.* [2009] values seem to be most consistent with ones obtained in this study. This result is not so surprising because *Mathew et al.* [2009] values were estimated from AMSR-E measurements, with the use of ice temperature regressed from near surface temperature of ERA-Interim data.

Due to the distinct contrast of emissivity across the boundary of multiyear ice (Figures 4 and 5), it is interesting to examine a possible means to use the retrieved emissivities for discriminating first-year ice from multiyear ice on a daily basis with a pixel-level resolution. The possibility stems from the change in ice optical properties with ice-type, due to changing salinity and therefore changing dielectric properties [*Vant et al.*, 1978]. It has been known that due to the dramatic decrease in salinity from first-year to multiyear sea ice, emissivity of multiyear sea ice is relatively low in comparison to the emissivity of first-year ice [*Vant et al.*, 1978; *Eppler et al.*, 1992; *Comiso*, 2012]. General spectral distributions shown in Figure 6 are consistent with earlier findings. All channels show almost the same general behavior regardless of polarization status, except for 10.65 GHz channel, in which the emissivity decrease is relatively small during the evolution into multiyear ice.

The emissivity slope noted between 10.65 GHz and 18.7 GHz is interesting; the emissivity slope for the first-year sea ice is opposite to that for the multiyear sea ice. The spectral slope change with time from the first-year to multiyear appears to be similar to what noted in other literatures [*Stroeve et al.*, 2006; *Mathew et al.*, 2009]. The spectrally opposite pattern of emissivity is more clearly shown in the vertical polarization than the horizontal polarization. It may be because horizontal polarization is more sensitive to the surface roughness, metamorphism, and sea ice salinity. Thus, vertical polarization is used to differentiate the first-year sea ice from multiyear sea ice. The feasibility of this conjecture is examined in detail in the following section.

4.2. Separating First-Year and Multiyear Sea Ice

In order to examine whether the slope change delineates the ice-type information, we define the vertically polarized emissivity difference (EVD) between 10.65 GHz and 18.7 GHz as

$$EVD = \varepsilon_V(10.65\,\text{GHz}) - \varepsilon_V(18.7\,\text{GHz}) \tag{4}$$

Before applying this EVD into the sea ice classification, we test whether uncertainty influences on the sign of EVD for multiyear sea ice. In order to examine the slope change that may be caused by uncertain elements of influencing the depletion/emission of the radiation, we calculated the range of slope by considering the largest uncertainties, after putting all uncertainty elements together. Emissivity differences between 10.65 and 18.7 GHz are computed with/without uncertainties, and then calculated slopes using two extreme cases: (1) largest positive error at 10.65 GHz with largest negative error at 18.7 GHz and (2) largest negative error at 10.65 GHz with largest positive error at 18.7 GHz. These two extreme results give an envelope of the slope delineating the slope range. Results indicated that the slope for the multiyear sea ice falls within a 0.0099–0.0452 range, still giving the worst case a positive sign. This suggests that the EVD method is solid.

In order to examine whether the EVD can be used for differentiating the sea ice-type from space, we estimate EVDs for 1 January 2010 and 1 January 2011, the two first Julian days separated by 1 year. Geographical distributions of the obtained EVD are shown in Figures 7a and 8a, along with NSIDC sea ice age distributions (Figures 7b and 8b), multiyear ice concentration from NASA Team algorithm (Figures 7c and 8c), and Norwegian OSI-SAF ice-type (Figures 7d and 8d).

On 1 January 2010, the NSIDC ice age shows multiyear sea ice mostly over the Central Arctic Ocean, Beaufort Sea, and in the western Greenland Sea. The corresponding EVD distribution shows that the positive EVD area is generally coincident with the multiyear sea ice area of NSIDC ice age data, while the negative area is in good agreement with the NSIDC first-year ice area. However, a certain degree of mismatch is found in the marginal ice zones such as the Bering Strait and the south coast of Greenland near the Denmark Strait, where positive signals exist on 1 January 2010 in spite of the first-year sea ice shown in the NSIDC data. In those marginal ice zones, EVD is likely contaminated by newly formed thin ice and/or open water, in particular during the winter [*Hwang et al.*, 2008]. Since the AMSR-E footprints for 10.65 GHz and 18.7 GHz are 29 km × 51 km
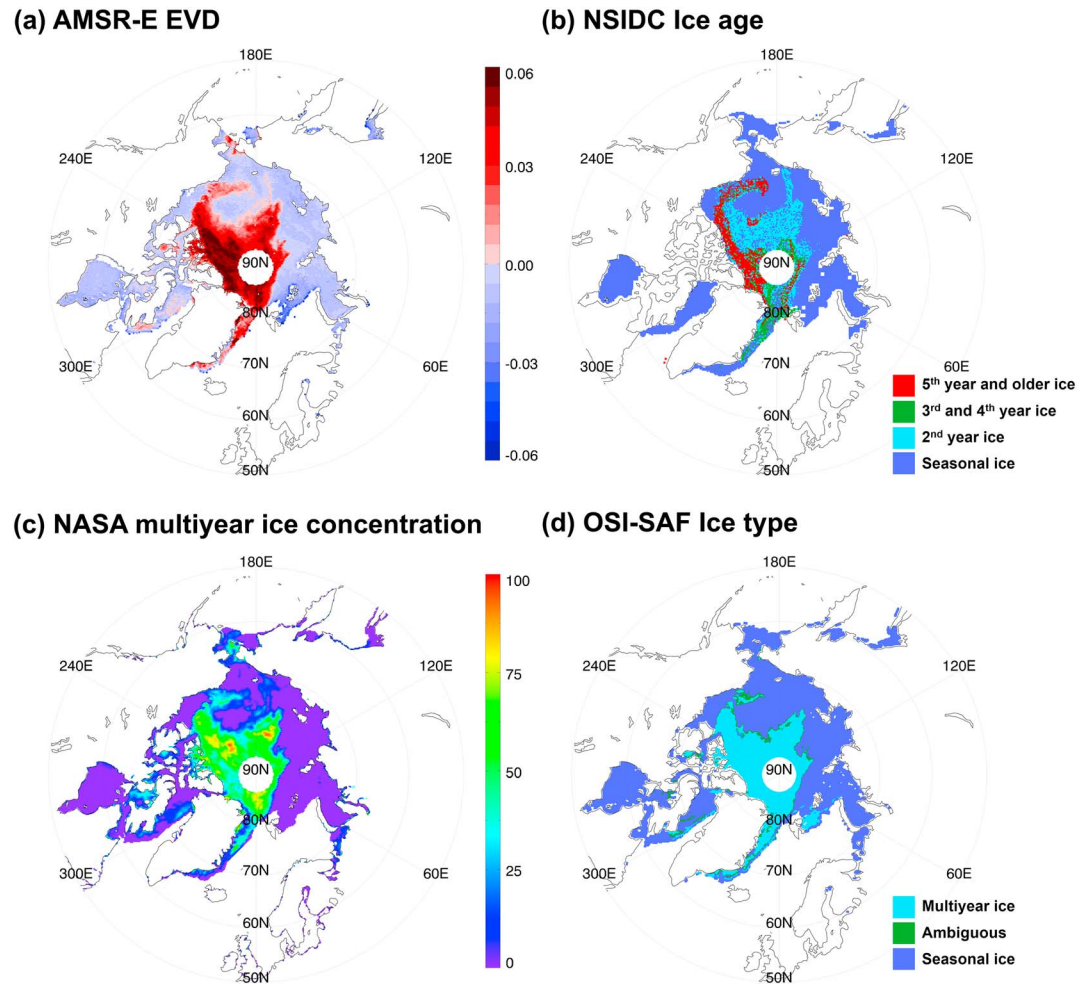
Figure 7. Geographical distributions of (a) the vertically polarized emissivity difference (EVD) between 10.65 and 18.7 GHz, (b) NSIDC sea ice age, (c) NASA Team multiyear ice concentration, and (d) OSI-SAF ice types over the Arctic on 1 January 2010.

and 16 km × 27 km, respectively, sea ice retrievals such as sea ice concentration in the marginal ice zones are likely to be subject to errors if there is pond-like water area or open water within the footprint. The current criteria of sea ice concentration >95% likely include such contamination effect in particular over the marginal ice zones.

The NASA Team multiyear ice concentration (Figure 7c) shows a distinct contrast between NSIDC first-year and multiyear ice, although the concentration of multiyear sea ice appears to be well below 100% over the most of region where the NSIDC product shows a multiyear sea ice.

The OSI-SAF ice product, which provides information of the sea ice region separated into seasonal, multiyear ice, and ambiguous area, seems to be in general agreeable to NSIDC first-year and multiyear ice areas. However, some detailed features including a horse-shoe shape distribution of multiyear ice over the Beaufort Sea are not clear.

Overall, except for the marginal ice zones, where sea ice is most likely first-year ice regardless of the EVD value, the EVD appears to be a good index to discriminate between first-year and multiyear sea ice, and a zero EVD value (separating the slope sign) can be used as a criterion as demonstrated in Figure 9. Furthermore, different from other approaches based on the statistical or tie-point algorithm, the EVD method is based on the use of physical properties that the sea ice undergoes a dielectric property changes associated with the salinity change of the ice with time. Such property change likely causes a spectral emissivity shape change with the ice age between 10.65 and 18.7 GHz.
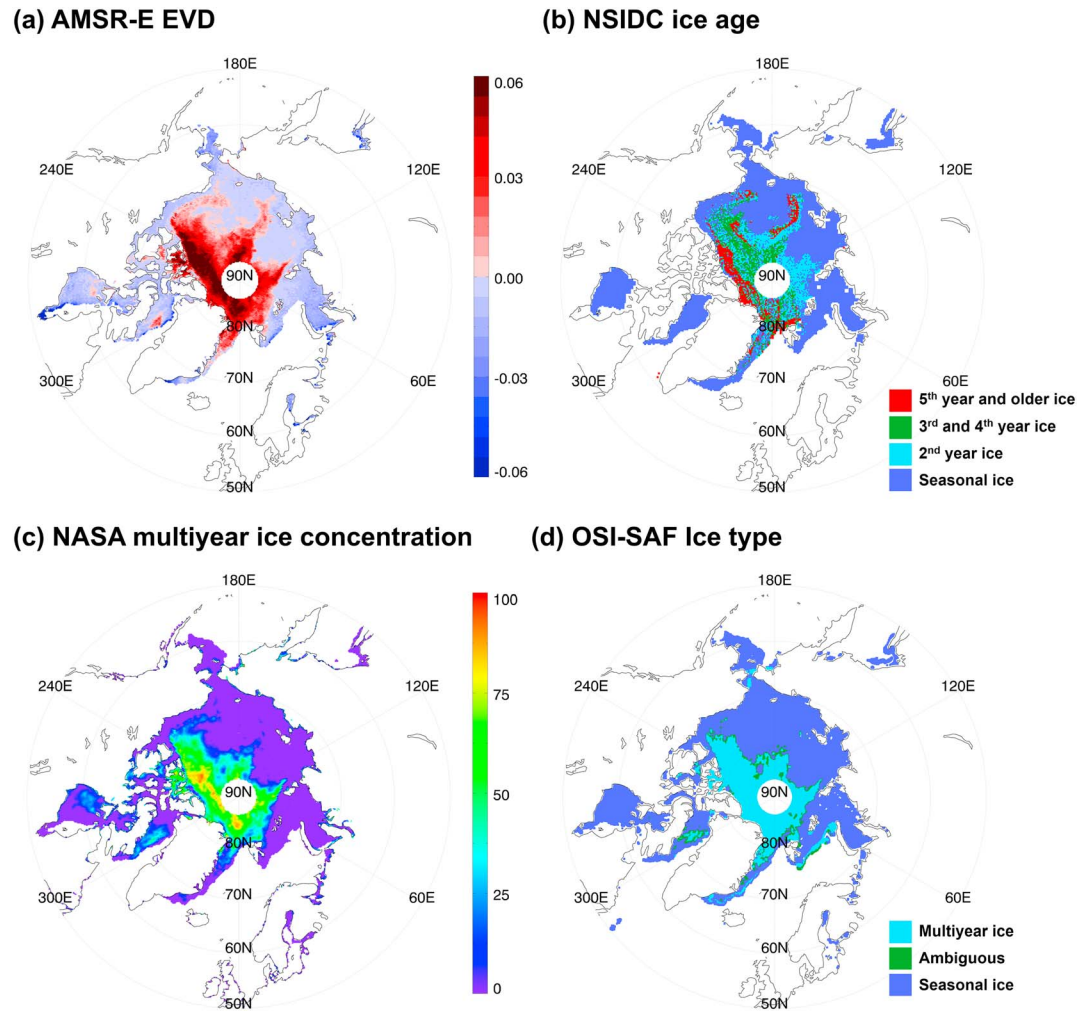
Figure 8. Same as in Figure 7 except for 1 January 2011.

The distributions of EVD and ice-type products are given for 1 January 2011, 1 year apart from 1 January 2010 (Figure 8). Compared with the distribution 1 year earlier, both EVD and NSIDC ice age indicate the multiyear sea ice expanding to 80°N toward the Barents Sea, and intruding toward the East Siberian Sea along about 150°E, and over the Beaufort Sea. Considering that NASA Team sea ice concentration and OSI-SAF ice-type results do not clearly depict such detailed patterns, conclusions are same as drawn for 1 January 2010 case.

4.3. Validation Against In Situ Ice-Type Reports

Validating the ice-type separation method using the EVD we use the ice-type information from CRREL IMB buoy data. When the buoy is installed over the ice, its type (first-year or multiyear sea ice) is reported. We collocate them with EVDs for January months during 2003–2011 period. Six tracks of drifting buoys are found and are plotted within the circles (Figure 9a). Initial deployment date and initial ice thickness for each buoy are provided in Table 5. For the collocation, once the location of CRREL IMB buoy is known at a particular time in January, all other ice age data for the nearest point are paired. However, considering that the buoy represents only a single point, while products are mainly based on microwave footprint measurements, matches may not be perfect unless the footprint of 25 km × 25 km is fully covered with the same type of ice. In order to ensure that CRREL buoy data represent multiyear ice or first-year ice we select collocations only if SIC = 100% over a 25 km × 25 km grid. Thus, the maximum distance between the buoy location and the 25 km × 25 km target center can be about 12.5 km. The initial ice thicknesses and the deployment dates, in addition to the SIC requirement, may assure that CRREL ice-type reports can be used for validating the satellite products, in spite of different representation between the point value and satellite's target value.
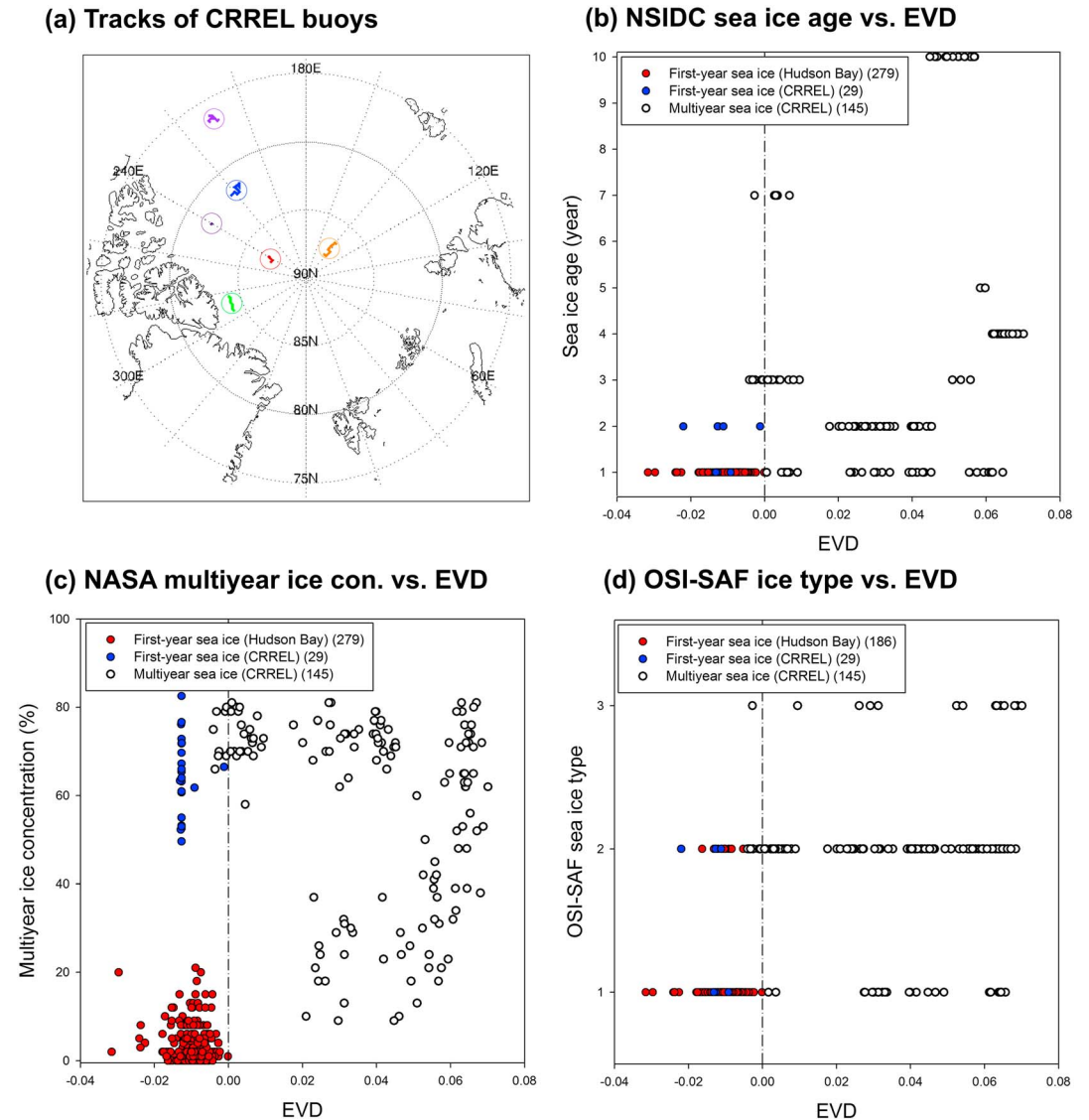
Figure 9. (a) Tracks of drifting buoys deployed on first-year ice (orange) and multiyear ice (other colors)—track locations are presented within the circles. (b) Scatterplots of CRREL multiyear ice (black circles) and first-year ice (blue dots), and first-year ice over the Hudson Bay (red dots) collocated with NSIDC ice age (*y* axis) and EVD (*x* axis). (c) Same as in Figure 9b except for EVD (*x* axis) and NASA Team multiyear ice concentration (*y* axis). (d) Same as in Figure 9b except of EVD (*x* axis) and OSI-SAF ice-type (in *y* axis; 1: first-year sea ice, 2: multiyear sea ice, and 3: ambiguous type). In Figure 9d 186 points for the Hudson Bay are due to the OSI-SAF data available from year 2006.

Beside the validation at the CRREL buoy locations, we use a point located in the middle of Hudson Bay (55.9°N, 277.3°E) where the ice-type is always first-year ice. Also compared against the EVDs and CRREL reports are NASA Team multiyear sea ice concentration and OSI-SAF ice-type data.

Table 5. Initial Deployment Dates and Ice Thickness of CRREL Buoys in Figure 9

Ice-Type	Buoy Tracks (in Figure 9a)	Initial Deployment Date	Initial Ice Thickness (cm)
Multiyear	Red	3 September 2005	258
	Purple	9 September 2006	290
	Black	9 September 2007	280
	Green	21 April 2008	204
	Blue	4 October 2010	182
First-year	Orange	30 September 2006	109

With these points in mind, comparison is made for CRREL IMB versus EVD and CRREL IMB versus NSIDC age (Figure 9b). A total of 145 multiyear sea ice (black open dots) and 29 first-year sea ice cases (blue dots) at CRREL IMB buoy locations are found, and 279 points of first-year sea ice cases (red dots) were obtained for Hudson Bay. Figure 9b shows that most of the CRREL multiyear ice points are located in the positive side of the EVD values (x axis). However, 8 points fall into negative sides (y axis) although the corresponding buoy data indicate multiyear sea ice. On the other hand, all of CRREL first-year sea ice falls in the negative side of EVD. Nearly all first-year ice points from the Hudson Bay are found on the negative side of EVD.

Also shown is the comparison of NSIDC sea ice age data (y axis) with CRREL IMB ice types. Figure 9b shows that the majority of black open dots (i.e., multiyear ice of the CRREL IMB type) are located in the area of NSIDC multiyear ice older than 1 year. However, some of the multiyear ice is determined to be first-year ice in the NSIDC data (black open dots on the first-year line of the y axis). The CRREL-determined first-year ice is located in the areas of both first-year and second-year ice (see the blue dots on one and two lines of the y axis). All ice identified as first-year sea ice in the Hudson Bay is without doubt first-year ice because there is no risk misidentifying isolated seasonal ice in south of the Arctic Circle using the ice-tracking method. Although the zero EVD criterion might not be robust enough to separate first-year ice from multiyear ice, the method seems to discriminate well between two types. Furthermore, this EVD method can be applied as long as brightness temperature is available at one geographical location and at one particular time, providing an opportunity to operationally monitor age-related sea ice variation or movement.

Also compared are EVDs against the NASA Team multiyear ice concentration and OSI-SAF ice-type, along with first-year and multiyear separation made by CRREL IMB data (Figures 9c and 9d). The matched points are same as in Figure 9b except for the Hudson Bay where OSI-SAF data are available from year 2006. Figure 9c shows that most of the CRREL multiyear ice points (black open dots) have a wide range of the concentration from 15% to 80%. On the other hand, CRREL-determined first-year ice points (blue dots) show the concentration ranging from 45% to 85%. The first-year sea ice over the Hudson Bay show multiyear sea ice concentration from 0% to 20%. From the comparison of NASA Team multiyear sea ice concentration with CRREL ice-type reports, it is concluded that there seems to be no clear link between two.

In the OSI-SAF ice types (1: first-year, 2: multiyear, 3: ambiguous), the CRREL multiyear sea ice points scatter from 1 to 3, although 71.2% are located in type 2 (multiyear). Similar scattered patterns are found in the CRREL first-year sea ice; about 35% of OSI-SAF first-year sea ice points are located in CRREL multiyear ice-type. No consensus seems to exist between OSI-SAF sea ice types and CRREL ice types.

Overall, from the comparison of AMSR-derived EVDs with CRREL observations of ice types, and against NASA Team multiyear ice concentration, and OSI-SAF ice-type, the ice-type separation is clearly better demonstrated in the EVDs. We claim that this more physics-oriented ice-type separation proposed in this study provides a good tool to discriminate between first-year and multiyear sea ice, at an instantaneous pixel scale.

5. Summary and Conclusions

In this study, polarized emissivities of the sea ice at the lower frequencies (here 10.65, 18.7, 23.8, and 36.5 GHz) have been retrieved over the Arctic in January. In this retrieval, a radiative transfer calculation was made for solving the surface emissivities with condition that (1) surface temperature is adopted from 6.9 GHz-retrieved sea ice temperature based on the Fresnel assumption and (2) atmospheric contributions are calculated using a radiative transfer model with ERA-Interim atmospheric profiles as inputs.

The geographical distributions of the retrieved emissivities from AMSR-E measurements over the Arctic Sea during January of 2003–2011 show that horizontally polarized emissivities are more complicated than the vertical component. Generally, lower emissivities are found in the region where multiyear ice is prevalent and lower emissivity regions have a clear contrast with higher values in the presumably first-year sea ice area. The spectral distributions of the retrieved emissivities in the 10.65–36.5 GHz range are well agreeable to what noted in other studies. However, it was shown that the retrieved emissivities for multiyear sea ice at 23.8 and 36.5 GHz are subject to substantial errors. Although this method has no difficulty to use for the first-year sea ice, the emissivity retrieval for the multiyear sea ice from 23.8 to 36.5 GHz measurements can be erroneous. It is due to the omission of freeboard ice scattering and the assumption of temperature emission layers same as

for 6.9 GHz. Sensitivity tests indicated that errors in the retrieved emissivity at 23.8 and 36.5 GHz can be up to 8% and 20%, respectively, while emissivity at frequencies below 18.7 GHz can be retrieved within a 2% error. But, more accurate retrievals can be possible when the freeboard ice scatterings and specific emission layers are taken into account for the multiyear sea ice.

It is noted that the spectral dependency of emissivity across the 10.65–18.7 GHz frequency bands appears opposite between the first-year and multiyear sea ice; the positive slope of emissivity between 10.65 and 18.7 GHz for first-year ice appears to change and reverse for multiyear sea ice. Based on such slope change, the vertically polarized emissivity difference (EVD) between 10.65 and 18.7 GHz was defined as an index of separating ice-type between first-year and multiyear ice. From the comparison of EVD with NSIDC tracking-based ice age data, it has been shown that two products are comparable, in terms of geographical distributions of the first-year and multiyear ice, except in some marginal ice zones where open water contamination is expected. The method has further been validated against ice-type information obtained at locations of CRREL IMB drifting buoys. It has been shown that a zero value of the AMSR-E based EVD can well separate first-year ice from multiyear ice across the Arctic.

References

Andersen, S. (1998), Monthly Arctic sea ice signatures for use in passive microwave algorithms, *Tech. Rep., 98-19*, Danish Meteorological Institute.

Andersen, S., R. Tonboe, L. Kaleschke, G. Heygster, and L. T. Pedersen (2007), Intercomparison of passive microwave sea ice concentration retrievals over the high-concentration Arctic sea ice, *J. Geophys. Res., 112*, C08004, doi:10.1029/2006JC003543.

Anderson, M., A. C. Bliss, and M. Tschui (2014), *MEaSUREs Arctic Sea Ice Characterization Daily 25 km EASE-GRID 2.0.*, NASA DAAC at Natl. Snow and Ice Data Cent., Boulder, Colo., doi:10.5067/MEASURES/CRYOSPHERE/nsidc-0532.001.

Breivik, L.-A., and S. Eastwood (2009), Upgrade of the OSI SAF sea ice edge and sea ice type products—Introduction of ASCAT. Tech. Rep., Norwegian Meteorological Institute.

Campbell, W. J., and P. Gloersen (1983), Report of the first Nimbus-7 SMMR experiment team workshop, NASA Tech. Memo. 85093, NASA Goddard Space Flight Center, Greenbelt, Md.

Cavalieri, D. J. J., P. Crawford, M. R. Drinkwater, D. T. Eppler, L. D. Farmer, R. R. Jentz, and C. C. Wackerman (1991), Aircraft active and passive microwave validation of sea ice concentration from the Defense Meteorological Satellite Program Special Sensor Microwave Imager, *J. Geophys. Res., 96*(C12), 21,989–22,008, doi:10.1029/91JC02335.

Comiso, J. C. (1983), Sea ice effective microwave emissivities from satellite passive microwave and infrared observation, *J. Geophys. Res., 88*(C12), 7686–7704, doi:10.1029/JC084iC09p05699.

Comiso, J. C. (1990), Arctic multiyear ice classification and summer ice cover using passive microwave satellite data, *J. Geophys. Res., 95*(C8), 13,411–13,422, doi:10.1029/JC095iC08p13411.

Comiso, J. C. (2012), Large decadal decline of the Arctic multiyear ice cover, *J. Clim., 25*, 1176–1193, doi:10.1175/JCLI-D-11-00113.1.

Comiso, J. C., D. J. Cavalieri, and T. Markus (2003), Sea ice concentration, ice temperature, and snow depth using AMSR-E data, *IEEE Trans. Geosci. Remote Sens., 41*(2), 243–252, doi:10.1109/TGRS.2002.808317.

Dee, D. P., et al. (2011), The ERA-interim reanalysis: Configuration and performance of the data assimilation system, *Q. J. R. Meteorol. Soc., 136*, 553–597, doi:10.1002/qj.828.

Eppler, D., et al. (1992), Passive microwave signatures of sea ice, in *Microwave Remote Sensing of Sea Ice*, edited by F. Carsey, pp. 47–71, AGU, Washington, D. C., doi:10.1029/GM068p0047.

Fowler, C., W. J. Emergy, and J. Maslanik (2004), Satellite-derived evolution of Arctic sea ice age: October 1978 to March 2003, *IEEE Geosci. Remote Sens. Lett., 1*(2), 71–74, doi:10.1109/LGRS.2004.824741.

Fowler, C., J. Maslanik, W. Emery, and M. Tschudi (2013), *Polar Pathfinder Daily 25 km EASE-Grid Sea Ice Motion Vectors-Version 2*, NSIDC, Boulder, Colo., doi:10.5067/O57VAIT2AYYY.

Francis, J. A., and S. J. Vavrus (2012), Evidence linking Arctic amplification to extreme weather in mid-latitudes, *Geophys. Res. Lett., 39*, L06801, doi:10.1029/2012GL051000.

Haggerty, J. A., and J. A. Curry (2001), Variability of sea ice emissivity estimated from airborne passive microwave measurements during FIRE SHEBA, *J. Geophys. Res., 106*(D14), 15,265–15,277, doi:10.1029/2000JD900485.

Hao, G., and J. Su (2015), A study of multiyear ice concentration retrieval algorithms using AMSR-E data, *Acta Oceanol. Sin., 34*(9), 102–109, doi:10.1007/s13131-015-0656-1.

Hwang, B. J., J. K. Ehn, and D. G. Barber (2008), Impact of ice temperature on microwave emissivity of thin newly formed sea ice, *J. Geophys. Res., 113*, C02021, doi:10.1029/2006JC003930.

Ivanova, N., et al. (2015), Inter-comparison and evaluation of sea ice algorithm: Toward further identification of challenges and optimal approach using passive microwave observation, *Cryosphere, 9*, 1797–1817, doi:10.5194/tc-9-1797-2015.

Jahn, A., et al. (2012), Late-twentieth-century simulation of Arctic sea ice and ocean properties in the CCSM4, *J. Clim., 25*, 1431–1451, doi:10.1175/JCLI-D-11-00201.1.

Jakobson, E., T. Vihma, T. Palo, L. Jakobson, H. Keernik, and J. Jaagus (2012), Validation of atmospheric reanalyses over the central Arctic Ocean, *Geophys. Res. Lett., 39*, L10802, doi:10.1029/2012GL051591.

Lee, S.-M., and B.-J. Sohn (2015), Retrieving the refractive index, emissivity, and surface temperature of polar sea ice from 6.9 GHz microwave measurements: A theoretical development, *J. Geophys. Res. Atmos., 120*, 2293–2305, doi:10.1002/2014JD022481.

Mätzler, C. (2006), *Thermal Microwave Radiation: Applications for Remote Sensing*, Inst. of Electr. Eng, London, UK.

Maslanik, J., J. Stroeve, C. Fowler, and W. Emery (2011), Distribution and trends in Arctic sea ice age through spring 2011, *Geophys. Res. Lett., 38*, L13502, doi:10.1029/2011GL047735.

Mathew, N., G. Heygster, and C. Melsheimer (2009), Surface emissivity of the Arctic sea ice at AMSR-E frequencies, *IEEE Trans. Geosci. Remote Sens., 47*(12), 4115–4124, doi:10.1109/TGRS.2009.2023667.

Perovich, D., B. Richter-Menge, B. Elder, T. Arbetter, K. Claffey, and C. Polashenski (2013), *Observing and Understanding Climate Change: Monitoring the Mass Balance, Motion, and Thickness of Arctic Sea Ice*, Report, Cold Reg. Res. And Eng. Lab., Hanover, N. H., [Available at http://imb.erdc.dren.mil.]

Polashenski, C., D. Perovich, J. Richter-Menge, and B. Elder (2011), Seasonal ice mass-balance buoys: Adapting tools to the changing Arctic, *Ann. Glaciol.*, *52*(57), 18–26, doi:10.3189/172756411795931516.

Sohn, B. J., and S.-M. Lee (2013), Analytical relationship between polarized reflectivities on the specular surface, *Int. J. Remote Sens.*, *34*(7), 2368–2374, doi:10.1080/01431161.2012.744490.

Stroeve, J. C., T. Markus, J. A. Maslanik, D. J. Cavalieri, A. J. Gasiewski, J. F. Heinrichs, J. Holmgren, D. K. Perovich, and M. Sturm (2006), Impact of surface roughness on AMSR-E sea ice products, *IEEE Trans. Geosci. Remote Sens.*, *44*(11), doi:10.1109/TGRS.2006.880619.

St. Germain, K. M. (1993), Application of spectral microwave radiometry to sensing of sea ice and the ocean surface, PhD dissertation, Univ. of Massachusetts.

Tonboe, R. T., and S. Andersen (2004), Modelled radiometer algorithm ice concentration sensitivity to variations of the Arctic sea ice snow cover, Sci. Rep. 04-03, Danish Meteorological Institute.

Tonboe, R. T., G. Dybkjær, and J. L. Høyer (2011), Simulations of the snow covered sea ice surface temperature and microwave effective temperature, *Tellus A*, *63A*, 1028–1037, doi:10.1111/j.1600-0870.2011.00530.x.

Vant, M. R., R. O. Ramseier, and V. Makios (1978), The complex dielectric constant of sea ice at frequencies in the range 0.1–40 GHz, *J. Appl. Phys.*, *49*, 1234–1280, doi:10.1063/1.325018.

Warren, S. G., I. G. Rigor, and N. Untersteiner (1999), Snow depth on Arctic sea ice, *J. Clim.*, *12*, 1814–1825.

Willmes, S., M. Nicolaus, and C. Haas (2014), The microwave emissivity variability of snow covered first-year sea ice from late winter to early summer: A model study, *Cryosphere*, *8*, 891–904, doi:10.5194/tc-8-891-2014.

Wu, B., and J. Wang (2002), Winter Arctic Oscillation, Siberian high, and East Asia winter monsoon, *Geophys. Res. Lett.*, *29*(19), 1897, doi:10.1029/2002GL015373.

Ye, Y., and G. Heygster (2015), Arctic multiyear ice concentration retrieval from SSM/I data using the NASA Team algorithm with dynamic tie points, in *Toward an Interdisciplinary Approach in Earth System Sciences*, edited by G. Lohmann et al., pp. 99–108, Springer, Cham, Switzerland.

Ye, Y., G. Heygster, and M. Shokr (2016), Improving multiyear ice concentration estimates with reanalysis air temperatures, *IEEE Trans. Geosci. Remote Sens.*, *54*(5), 2602–2614, doi:10.1109/TGRS.2015.2503884.

Zhang, S., J. Zhao, K. Frey, and J. Su (2013), Dual-polarized ratio algorithm for retrieving Arctic sea ice concentration from passive microwave brightness temperature, *J. Oceanogr.*, *69*, 215–227, doi:10.1007/s10872-012-0167-z.